

pubs.acs.org/JPCL Letter

# Formation and Luminescence of Single Oxygen Impurities on the Surface of SiC Nanocrystals

Joseph D. Granlie, Erik K. Hobbie, and Dmitri S. Kilin\*



Cite This: J. Phys. Chem. Lett. 2023, 14, 6202-6208



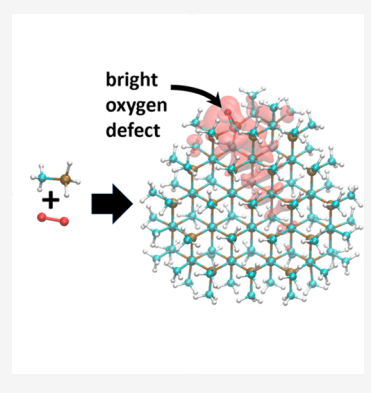
ACCESS I

III Metrics & More

Article Recommendations

Supporting Information

ABSTRACT: Impurities that hinder luminescence are a common problem in the synthesis of nanocrystals, and controlling the synthesis reaction could provide a way to avoid or use impurities beneficially. Excited state molecular dynamics is used to determine how oxygen impurities appear in the plasma synthesis of silicon carbide nanocrystals (SiC NCs). Formation of impurities is studied by considering the intermediate structures in the simulated photoreaction. The results show the most probable bonding patterns of silicon, carbon, and oxygen. These intermediates are used as a basis for studying the luminescence of expected oxygen impurities in SiC NCs, where luminescence is studied by first-principles modeling and density matrix dissipative dynamics based on on-the-fly non-adiabatic couplings and the Redfield tensor. Modeling the dissipation of energy from electronic to nuclear degrees of freedom reveals multiple impurities with significant photoluminescence quantum yields.



Bulk silicon carbide (SiC) offers several physical properties that could make it useful in modern technology, 1-5 much like silicon-based electronics. Such properties include a higher electric breakdown field, a higher carrier saturation velocity, a higher thermal conductivity, and a wider bandgap compared to those of bulk silicon. Despite this, the synthesis and manufacture of SiC present a challenge. The strong covalent bonds of SiC contribute to its hardness and brittleness, complicating sintering<sup>6-8</sup> and machining<sup>9</sup> processes. A colloidal nanocrystal (NC) ink could address these issues and offer an efficient processing technique for SiC materials such as coatings and layered electronics. Recent work toward producing SiC NCs has been based on plasma synthesis. 10 Depending on the process used, atmospheric contaminants can cause significant impurities. Moreover, the effects of such impurities on the photoluminescence (PL) and surface chemistry of SiC NCs are still not well understood. 11-14 A deeper understanding of how impurities affect the physical and electronic properties of SiC NCs could aid in the development of new systems tuned to achieve the desired emission wavelength.

A challenge is posed by the characterization of impurities that can be found in SiC NCs produced via plasma photoreaction. On the surface of NCs, oxygen is expected to act as a nonradiative recombination site and quench PL. <sup>15,16</sup> However, experiments have shown that oxygen impurities can be bright in the case of SiC NCs. <sup>11,17</sup> The formation of impurities in NCs and their characterization call for two types of computational simulations. Modeling of plasma-assisted NC formation requires the study of excited state molecular dynamics. Computational methods such as NEXMD<sup>18</sup> and

time-dependent density functional tight-binding theory 19 have been used to explore a similar class of problems. There have been several approaches to modeling photoreactions, including thermal molecular dynamics (MD), in which the nuclei's velocities are scaled linearly to the desired temperature and the electronic configuration remains in the ground state, and excited state molecular dynamics (ESMD), in which the electronic configuration is initially excited, and the transition energy drives the reaction. Another available approach is based on ab initio molecular dynamics and density functional theory (DFT), using a time-dependent excited state molecular dynamics (TDESMD) approach to study the photoreaction.<sup>20</sup> In the TDESMD algorithm, the excitation and de-excitation of electrons in a laser field are treated as stepwise transitions rather than sinusoidal, inspired by merging ideas of Rabi oscillations<sup>21,22</sup> and surface hopping approximation.<sup>23</sup> A comparison of MD, ESMD, and TDESMD has been performed previously.<sup>24</sup> There, it was reported that both MD and ESMD failed to reproduce a substantial portion of the intermediates and products found experimentally. However, TDESMD was found to agree with experiment the best and showed the importance of electronic oscillations in determining the reaction pathway. TDESMD allows the exploration of the potential energy surface (PES) in the sense of an "on-the-

Received: May 1, 2023 Accepted: June 6, 2023 Published: June 29, 2023





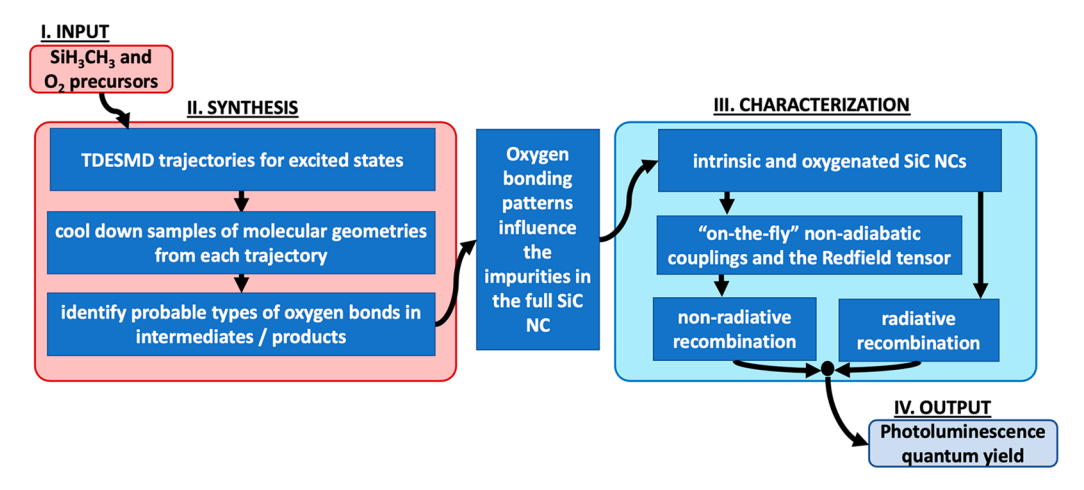


Figure 1. Schematic diagram summarizing the protocol used. The input and outputs of each step are shown in rounded boxes. Formation is the first stage (left) and involves extracting oxygen bonding patterns from intermediates found in TDESMD. The oxygen bonding patterns from TDESMD are expected to influence the impurities found in the fully formed SiC NC. Assessing photoluminescence is the second stage (right) and involves computing the Redfield tensor so that nonradiative electron dynamics can be investigated to provide the photoluminescence quantum yield for each model.

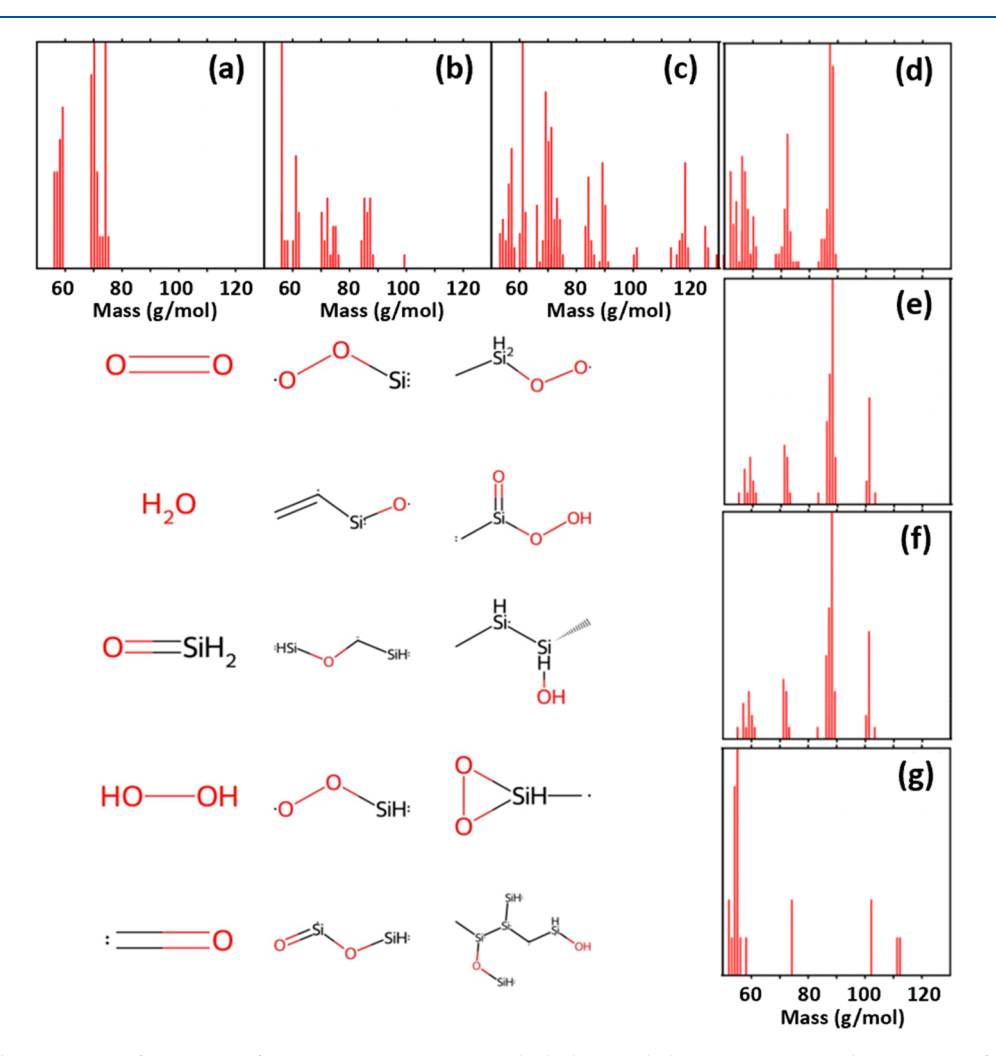


Figure 2. Simulated mass spectra for a series of TDESMD trajectories in which the initial electronic excitation has energies of (a) 3.12, (b) 6.54, (c) 6.76, (d) 7.32, (e) 7.71, (f) 7.86, and (g) 17.12 eV. The height of each bar represents the number of times an intermediate of that mass appeared along the TDESMD trajectory. Precursors  $SiH_3CH_3$  (46.1438 g/mol) and  $O_2$  (31.9988 g/mol) are not shown so we can focus on the formation of larger intermediates. The inset shows a sample of the intermediates found along the 7.3224 eV TDESMD trajectory. Duplicates have been omitted. The single dots on some of the intermediates indicate unbonded electrons.

Table 1. Number of Intermediates and Types of Oxygen Bonding for Seven Different TDESMD Initial Excitation Energies<sup>a</sup>

excitation energy (eV)	no. of intermediates	Si-O	C-O	Si-O-H	С-О-Н	Si-O-Si	Si-O-C	C-O-C
3.1173	31	8	3	7	2	0	0	0
6.5387	40	10	5	4	1	0	0	0
6.7605	73	42	15	10	2	7	1	0
7.3224	41	19	2	2	0	2	1	0
7.7099	28	8	3	3	0	0	2	0
7.8564	76	33	12	10	2	2	0	0
17.1167	19	1	7	0	0	0	0	0

"Columns 3 and 4 give the number of times oxygen bonded to silicon and carbon, respectively, in the geometry-optimized intermediates. Columns 5–9 give the number of times oxygen bonded to a specific combination of silicon and carbon. For instance, the table shows that for the 3.1173 eV TDESMD trajectory, oxygen bonded to silicon and hydrogen (forming a silicon—oxygen—hydrogen chain) seven times. We notice that in all but one case, oxygen predominately bonded to silicon and formed a Si—O—H chain. Additional details are provided in SI Table S1.

fly" trajectory. Specifically, the TDESMD trajectory explores the local region of phase space where the curvature of the PES determines the forces and direction of the next increment in phase space. This results in the trajectory exploring and converging toward different local minima of phase space. Our group has applied TDESMD to study the photofragmentation of tetranitromethane, 25 lanthanum complexes, 20,24,26 polymers,<sup>27</sup> and the photopolymerization of cyclohexasilane<sup>28</sup> and found agreement with experimental results. Characterization of impurities in NCs requires the comparison of ground state and dynamic electronic properties. Ground state properties such as the bandgap and charge distribution can be assessed using DFT. Electron dynamics properties can be characterized by the photoluminescence quantum yield, which requires comparison of radiative and nonradiative pathways of excited state recombination.<sup>29</sup> The study of nonradiative relaxation requires coupling electronic degrees of freedom to nuclear degrees of freedom, which has been addressed by nonadiabatic molecular dynamics. 30-32 Another approach is based on Redfield theory, in which electronic-nuclear coupling is assumed to be weak. 33-35 The Redfield tensor, which controls the nonradiative relaxation rates of excited states, can be calculated using ground state molecular dynamics. This scheme has been implemented previously, and there is reasonable agreement with experimental results. 29,36

In this work, we study the photoreaction of SiH<sub>3</sub>CH<sub>3</sub> and O<sub>2</sub> to better understand interfacial oxygen impurities that might be found during the production of SiC NCs. This work applies the TDESMD algorithm to large molecule formation rather than photofragmentation, which addresses a new challenge and covers a broader range of processes. Simulating the full crystallization of SiC NCs is tremendously computationally expensive, and this difficulty may be avoided by connecting the reaction intermediates to products. To accomplish this goal, we follow the protocol sketched in the schematic diagram shown in Figure 1. Here we provide a brief description of the methods, while a detailed account of the implementation of TDESMD and application of Redfield theory to assess nonradiative electronic relaxations can be found in the Supporting Information. We begin by considering the ensemble of precursors, SiH<sub>3</sub>CH<sub>3</sub> and O<sub>2</sub>, and identifying their most likely absorption transitions based on oscillator strength. The TDESMD algorithm, based on concepts of Rabi oscillations and surface hopping, is performed for a set of the seven most probable excitations. For each TDESMD trajectory, snapshots of the molecular geometries at certain time steps are geometry-optimized<sup>28</sup> to account for cooling after exiting the plasma reactor. OpenBabel<sup>37</sup> is used to extract

each intermediate molecule from the TDESMD simulation cell, which allows the simulated mass spectra to be computed.<sup>24</sup> In addition, SMARTS queries<sup>38</sup> are used to reduce the intermediate molecular structures into the number and type of oxygen bonds formed during the trajectory. Specifically, we count the number of times oxygen bonds to silicon, carbon, and/or hydrogen. We adopt a shorthand to refer to these bonds; for example, an oxygen bonded to silicon is termed Si-O. The Si-O, C-O, Si-O-H, C-O-H, Si-O-Si, Si-O-C, and C-O-C bonds were considered. By determining the most common bonding patterns of oxygen, we can predict the likely morphology of oxygen impurities on the surface of SiC NCs. Oxygen atoms are expected to lie on the surface of the NC due to their bonding nature. Next, the luminescent properties of pure (intrinsic) SiC NC and several NC models with single oxygen impurities were studied using Redfield theory. We chose to study the oxygen impurities predicted by TDESMD and a few more hypothetical impurities. Using a molecular dynamics trajectory, nonadiabatic couplings were computed "on the fly" and used to construct the Redfield tensor, where the electronic transitions are facilitated by thermal nuclear motion and are accounted for perturbatively up to second order in coupling. Following the dissipative Redfield equation of motion, the nonradiative relaxation of electronic states could be considered. Via combination of the rates of nonradiative transition and the radiative recombination, computed via Einstein's coefficients, the photoluminescence quantum yield was calculated for each impurity.

The results of TDESMD were first analyzed using simulated mass spectra. Figure 2 shows the simulated mass spectra for each of the seven excitations performed. Our chosen precursors, SiH<sub>3</sub>CH<sub>3</sub> and O<sub>2</sub>, have molar masses of 46.1438 and 31.9988 g/mol, respectively. The mass spectra show a consistent formation of intermediates larger than the precursors and the early formation of SiC NCs. In six of the excitations, we see peaks just above 70 g/mol and five of the excitations show peaks between 80 and 90 g/mol. Due to the rapid adsorption and desorption of hydrogen, all peaks are largely broadened. This causes the intermediates to have extremely variable molecular geometries, so we must analyze the intermediates using a different method.

With the goal of extracting information about oxygen bonding in a fully formed SiC NC, intermediates that do not include an oxygen atom are ignored. It should be noted that because only the early reaction intermediates are calculated, which are tiny molecules in comparison to the full NC, our method does not observe any other crystal defects such as

vacancies or substitutions. A sample of oxygen-containing intermediates is shown in Figure 2 (inset). Due to the high variance in the molecular geometry of intermediates, we must diverge from considering the likelihood of any specific intermediate forming. Typically, the thermodynamic stability of competing intermediate isomers could be assessed by their total energy. One could build a ranked table of intermediates, by identifying the total energy, which would be ordered by the Boltzmann probability. Such a table would show which intermediates are most energetically favorable. Another approach for assessing thermodynamic stability, which we adopt, is rooted in the ergodic hypothesis. The TDESMD trajectory deals with a simulation cell containing several competing intermediates at a given time. On the basis of the ergodic hypothesis, less stable intermediates will have a shorter lifetime while more stable intermediates will have a longer lifetime. Thus, the frequency of appearance of a given intermediate along a trajectory and the relative height of the relevant peak in the mass spectra are proportional to its stability. We extend the idea of stable intermediates to the stability of certain oxygen bonds. Specifically, we consider the number and type of bonds formed by oxygen rather than the number of times any specific fragment was formed. This bond information is presented in Table 1. On the basis of the ergodic hypothesis, we assume that a sufficiently long trajectory will cover the most important and voluminous regions of phase space. Thus, the most probable bonding configurations will be those that appear most frequently over the trajectory and will be the same bonds frequently seen in real-world reactions. We notice a very strong trend of siliconoxygen bonding and a silicon-oxygen-hydrogen chain being the most prevalent in all excitations. To make the transition from the TDESMD intermediates to a fully formed SiC NC, we hypothesize that the oxygen will end up on the surface of the NC rather than as a crystal defect. This transition is rationalized due to the bonding nature of oxygen. Because oxygen typically forms only two bonds, it is reasonable to expect that once it bonds to silicon and/or carbon, the rest of the NC will form starting from the silicon and/or carbon atoms; the oxygen would act as a nucleation site for the crystal. On this basis, we can use the information in Table 1 to predict the impurities in a fully formed SiC NC. This would lead to SiOH being the most likely impurity. In this study, for the sake of completeness, we consider a wider range of impurities.

We assume formation of a range of O-doped models. Most representative examples of the six SiC NC models are shown in Figure 3, and we investigate the electronic structure and the electron dynamics and photoluminescence in these models. The DOS was calculated for each of the SiC NCs and is shown in Figure 3. Apart from SiOC, the studied defects show very little change in bandgap. Moreover, all defects show little change in the structure of the DOS. We notice that COH and SiOH create significant gaps at 2 eV, while SiOCH<sub>3</sub> and SiOH decrease the degeneracy of the LUMO state slightly. In the case of SiOC, we see the creation of a new HOMO with very little degeneracy and a significant change in the conduction band structure. The low degeneracy of the SiOC HOMO is expected to significantly decrease the PL.

Next, we consider the partial charge densities of each SiC NC model, as shown in Figure 4. Due to the electronegativity of oxygen, it is expected that the frontier orbitals of a NC will localize around the oxygen atom. Surprisingly, we do not see the expected localization in any of the oxygen impurities except

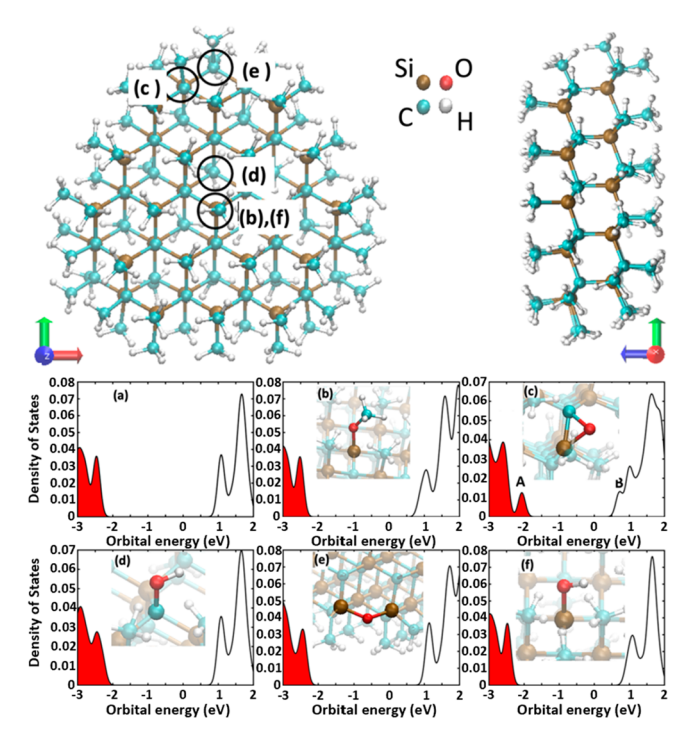
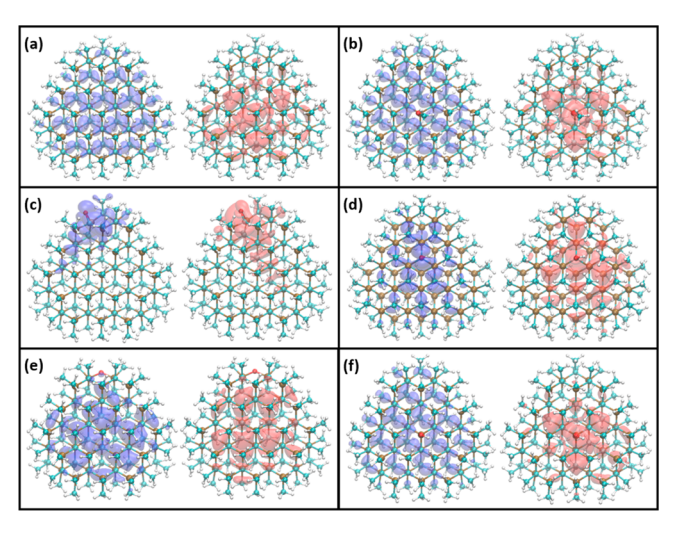


Figure 3. Intrinsic SiC NC model and the five studied impurities. The top inset shows the intrinsic model. The model contains 326 atoms, is 16.14 Å in diameter, and is simulated in a 22.6 Å  $\times$  22.4 Å  $\times$  13.4 Å unit cell. Circles and lettering signify the locations of the five impurities: (b) SiOCH<sub>3</sub>, (c) SiOC, (d) COH, (e) SiOSi, and (f) SiOH. Silicon, oxygen, carbon, and hydrogen atoms are shown as brown, red, cyan, and white spheres, respectively. Labeled panels show the density of states of the geometry-optimized SiC NC models, where the valence band is shaded red and the conduction band is white. Panels show the following models: (a) intrinsic, (b) SiOCH<sub>3</sub>, (c) SiOC, (d) COH, (e) SiOSi, and (f) SiOH. The DFT-calculated bandgaps are (a) 3.51, (b) 3.40, (c) 2.78, (d) 3.33, (e) 3.51, and (f) 3.42 eV. It is important to note that in panel c we see that SiOC narrows the bandgap by creating a new low-degeneracy HOMO and adds several states in the conduction band, signified by peaks A and B, respectively.

for SiOC. This could be due to SiOC being placed on the edge of the NC, as opposed to the SiOCH<sub>3</sub>, COH, and SiOH impurities. However, SiOSi is also an edge impurity so the location of the impurity cannot be the only factor determining the localization.

Finally, we consider the PL of the intrinsic and impure SiC NCs. We first look at the relaxation dynamics of the most probable transitions based on oscillator strength, where the intrinsic and SiOH dynamics are shown in Figure 5 (left) and all of the other models are shown in Figure S1. In all cases, we observe that the brightest transition, by an order of magnitude or more, is the LU  $\rightarrow$  HO transition. This allows us to continue assessing PL by assuming, following Kasha's rule, that the luminescence of each model mainly comes from the bandgap transition. We use eq S17 to calculate the PLQY, seen in Table 2. It is significant to note that the intrinsic, SiOCH<sub>3</sub>, and SiOH models all have similar PLQYs (55.37%, 41.49%, and 40.15%, respectively). PL over the MD trajectory is seen in Figure 5 (right). In agreement with the computed bandgaps, all models other than SiOC emit near 400 nm. In addition, we see that SiOC experiences the most thermal broadening.

In this study, we applied the TDESMD algorithm to study the photoreaction of  $SiH_3CH_3$  and  $O_2$  with the intention of



**Figure 4.** Orbital charge density of the HO (left, blue) and LU (right, red) energy levels for each of the SiC NC models: (a) intrinsic, (b) SiOCH<sub>3</sub>, (c) SiOC, (d) COH, (e) SiOSi, and (f) SiOH. The isosurface is visualized at  $0.006 \ e/a^3$ , where a is the Bohr radius. All models show little to no charge localization around the oxygen impurity when compared to the intrinsic model except for SiOC.

predicting oxygen impurities found in a full SiC NC. The results of TDESMD showed that silicon—oxygen bonding was more abundant than carbon—oxygen bonding. We found the most abundant pattern of oxygen bonding to be a silicon—oxygen—hydrogen chain. This is evidence of the most likely oxygen impurity that would appear on the SiC NC surface, as the oxygen atom will act as a nucleation point for the rest of the NC. We then studied the PL of SiC NCs with and without oxygen impurities. It is generally expected that an oxygen impurity will quench the luminescence of a NC. However, we found that the intrinsic, SiOCH<sub>3</sub>, and SiOH models all had similar PLQYs between 40% and 60%.

Experimental synthesis of SiC NCs typically produces NCs between 2 and 4 nm in diameter, while our simulated models are  $\sim$ 1.6 nm in diameter. While the sizes between the experiment and simulation differ, we expect the qualitative

Table 2. PLQYs and Relaxation Rates for the HO-LU Transition of Each SiC NC Model<sup>a</sup>

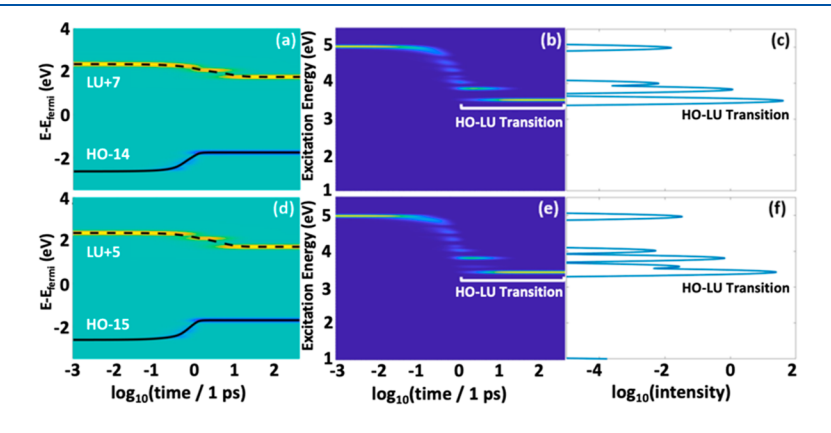
model	PLQY (%)	$K_{\rm nr}~({\rm fs}^{-1})$	$K_{\rm r}~({\rm fs}^{-1})$
intrinsic	55.37	$3.4140 \times 10^{-7}$	$4.2348 \times 10^{-7}$
SiOCH <sub>3</sub>	41.49	$3.4002 \times 10^{-7}$	$2.4111 \times 10^{-7}$
SiOH	40.15	$3.6464 \times 10^{-7}$	$2.4464 \times 10^{-7}$
СОН	19.43	$1.0506 \times 10^{-6}$	$2.5331 \times 10^{-7}$
SiOSi	16.80	$8.6744 \times 10^{-7}$	$1.7521 \times 10^{-7}$
SiOC	7.69	$1.3844 \times 10^{-4}$	$1.1529 \times 10^{-5}$

"The nonradiative transition rate,  $K_{\rm nr}$ , is the element of the Redfield tensor corresponding to the HO–LU transition. The radiative rate,  $K_{\rm rr}$  is calculated from Einstein's spontaneous emission coefficient. We note that SiOCH<sub>3</sub> and SiOH have PLQYs very similar to that of the intrinsic model due to the miniscule variation in  $K_{\rm nr}$ .

trends to remain the same. Specifically, in an experiment we would still expect to see NCs with SiOCH<sub>3</sub> and SiOH surface impurities emit with a PLQY similar to that of a pure SiC NC. Moreover, on a larger NC, a single oxygen atom should localize charge even less, so we may expect an even higher PLQY in experiments.

In our models, we chose to use methyl groups as ligands and performed calculations in a vacuum to decrease the computational expense. However, experimental ligands are generally much longer alkyl chains, and the NCs are not in a vacuum. We found that the most emissive HOMO and LUMO states were not surface states. Therefore, if the NC were in solution and surrounded by larger ligands, the interaction between solvent and NC electronic states would be minimal, and we would expect the electronic properties to resemble the simulation results.

Here, we have studied oxygen impurities in SiC NCs from photochemical and photophysics perspectives. The TDESMD algorithm was applied to investigate the mechanism of chemical formation of oxygen impurities in SiC NCs. To that end, multiple electronic excitations leading to different nuclear trajectories were used to explore the gas phase reaction of SiH<sub>3</sub>CH<sub>3</sub> and O<sub>2</sub>. Analysis of geometry-optimized intermediates showed that silicon—oxygen bonds were more



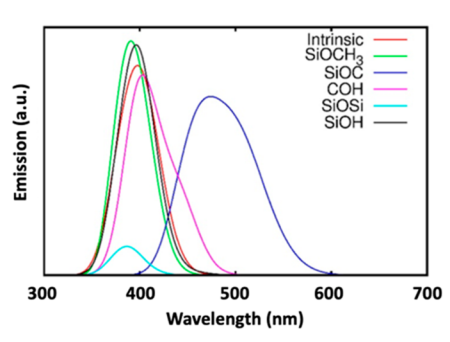


Figure 5. Electronic relaxation dynamics after initial high-oscillator strength excitation. Panels a—c show the intrinsic model. Panels d—f show the SiOH model. Panels a and d show the relaxation of the electron (yellow) and hole (blue). Dashed and solid black lines show the expected value of charge during relaxation. Panels b and e show the time-resolved emission spectra. Colors correspond to the intensity of the transition from blue (zero intensity) to yellow (largest intensity). Panels c and f show the time-integrated emission. The HO—LU transition is signified, and we see that in both cases it is the most intense emission by orders of magnitude. The right-most panel shows the simulated PL emission of the HO—LU transition for each SiC NC model during MD with a temperature of 300 K and a duration of 1000 fs. The vertical axis gives the intensity of emission, which is based on oscillator strength. In agreement with computed bandgaps, SiOC emits at a longer wavelength of ~490 nm and all other models emit at ~400 nm. The width of the peak for SiOC shows that it experiences the most thermal broadening.

prevalent than carbon—oxygen bonds, especially a silicon—oxygen—hydrogen chain. We extrapolate this to an expectation of the specific patterns of oxygen impurities binding to silicon and carbon in a fully formed SiC NC. We find that SiOH is the most likely intermediate produced in all TDESMD excitations, and we expect it to be abundant in fully formed SiC NCs.

The investigation of PL from various oxygen impurities was carried out using first-principles modeling and density matrix dissipative dynamics, governed by the Redfield equation of motion. We found that the intrinsic model has the highest PLQY of 55.37%. In general, oxygen is expected to localize at frontier orbitals and quench the PLQY. However, we found that the surface oxygen impurities SiOCH<sub>3</sub> and SiOH had PLQYs of 41.49% and 40.15%, respectively. The high PLQYs of SiOCH<sub>3</sub> and SiOH are rationalized by the very low degree of charge localization near the oxygen impurity, which results in a minimal change ni the nonradiative transition rate compared to that of the intrinsic model. As oxygen can be difficult to avoid in the synthesis of SiC NCs, the natural tendency of SiOH to form could be leveraged to be beneficial rather than detrimental for luminescence.

#### ASSOCIATED CONTENT

#### **Supporting Information**

The Supporting Information is available free of charge at https://pubs.acs.org/doi/10.1021/acs.jpclett.3c01182.

Additional figures and a detailed description of TDESMD and Redfield methodology (PDF)

Animated movie of representative TDESMD trajectory (MPG)

Animated movie of computed reaction intermediates stemming from TDESMD trajectory (MOV)

#### AUTHOR INFORMATION

#### **Corresponding Author**

Dmitri S. Kilin – Department of Chemistry and Biochemistry, North Dakota State University, Fargo, North Dakota S8108, United States; orcid.org/0000-0001-7847-5549; Email: Dmitri.kilin@ndsu.edu

#### Authors

Joseph D. Granlie — Department of Physics and Department of Mathematics, North Dakota State University, Fargo, North Dakota 58108, United States; orcid.org/0009-0008-2905-9336

Erik K. Hobbie – Department of Physics, North Dakota State University, Fargo, North Dakota \$8108, United States

Complete contact information is available at: https://pubs.acs.org/10.1021/acs.jpclett.3c01182

#### Notes

The authors declare no competing financial interest.

#### ACKNOWLEDGMENTS

This research is supported by National Science Foundation Grant 1944921. D.S.K. thanks S. Kilina, S. Tretiak, O. Prezhdo, D. Micha, and B. Rasulev for stimulating discussions. This research used resources of the National Energy Research Scientific Computing Center (NERSC), a U.S. Department of Energy Office of Science User Facility located at Lawrence Berkeley National Laboratory, operated under Contract DE-AC02-05CH11231 using allocation award m1251 for 2023,

"Computational Modeling of Photo-catalysis and Photo-induced Charge Transfer Dynamics on Surfaces". J.D.G. thanks Y. Han and M. Ericson for practical suggestions on TDESMD and data processing. The authors also thank A. Forde, Y. Han, L. Johnson, A. Flesche, K. N. Keya, S. Ghazanfari, M. Ericson, H. Griffin, A. Arshad, W. Tupa, and P. Adeoye for discussion and editorial suggestions.

#### REFERENCES

- (1) Elasser, A.; Chow, T. P. Silicon Carbide Benefits and Advantages for Power Electronics Circuits and Systems. *Proc. IEEE* **2002**, *90* (6), 969–986
- (2) Maboudian, R.; Carraro, C.; Senesky, D. G.; Roper, C. S. Advances in Silicon Carbide Science and Technology at the Microand Nanoscales. *J. Vacuum Sci. & Technol. A* **2013**, 31 (5), No. 050805.
- (3) Nair, V.; Yi, J.; Isheim, D.; Rotenberg, M.; Meng, L.; Shi, F.; Chen, X.; Gao, X.; Prominski, A.; Jiang, Y.; et al. Laser Writing of Nitrogen-Doped Silicon Carbide for Biological Modulation. *Sci. Adv.* **2020**, *6* (34), eaaz2743.
- (4) Harris, C. I.; Savage, S.; Konstantinov, A.; Bakowski, M.; Ericsson, P. Progress Towards SiC Products. *Appl. Surf. Sci.* **2001**, *184* (1), 393–398.
- (5) Chen, Y.; Zhang, X.; Xie, Z. Flexible Nitrogen Doped SiC Nanoarray for Ultrafast Capacitive Energy Storage. *ACS Nano* **2015**, 9 (8), 8054–8063.
- (6) Magnani, G.; Sico, G.; Brentari, A.; Fabbri, P. Solid-State pressureless sintering of silicon carbide below 2000°C. *J.European Ceram. Soc.* **2014**, 34 (15), 4095–4098.
- (7) Raju, K.; Yoon, D.-H. Sintering Additives for SiC Based on the Reactivity: A Review. Ceram. Int. 2016, 42 (16), 17947–17962.
- (8) Zapata-Solvas, E.; Bonilla, S.; Wilshaw, P. R.; Todd, R. I. Preliminary Investigation of Flash Sintering of SiC. *J. European Ceram. Soc.* **2013**, 33 (13), 2811–2816.
- (9) Goel, S. The Current Understanding on the Diamond Machining of Silicon Carbide. J. Phys. D: Appl. Phys. 2014, 47 (24), 243001
- (10) Petersen, R. J.; Thomas, S. A.; Anderson, K. J.; Pringle, T. A.; May, S.; Hobbie, E. K. Silicon-Carbide Nanocrystals from Nonthermal Plasma: Surface Chemistry and Quantum Confinement. *J. Phys. Chem. C* **2022**, *126* (30), 12935–12943.
- (11) Beke, D.; Jánosi, T. Z.; Somogyi, B.; Major, D. Á.; Szekrényes, Z.; Erostyák, J.; Kamarás, K.; Gali, A. Identification of Luminescence Centers in Molecular-Sized Silicon Carbide Nanocrystals. *J. Phys. Chem. C* **2016**, *120* (1), 685–691.
- (12) Castelletto, S.; Almutairi, A. F. M.; Thalassinos, G.; Lohrmann, A.; Buividas, R.; Lau, D. W. M.; Reineck, P.; Juodkazis, S.; Ohshima, T.; Gibson, B. C.; et al. Fluorescent Color Centers in Laser Ablated 4H-SiC Nanoparticles. *Opt. Lett.* **2017**, *42* (7), 1297–1300.
- (13) Dai, D.; Zhang, C.; Wang, L.; Wang, Y.; Zhang, B.; Deng, K.; Lu, W.; Fan, J. Reversible/Irreversible Photobleaching of Fluorescent Surface Defects of SiC Quantum Dots: Mechanism and Sensing of Solar UV Irradiation. *Adv. Mater. Interfaces* **2019**, *6* (11), 1900272.
- (14) Haq, A. U.; Buerkle, M.; Askari, S.; Rocks, C.; Ni, C.; Švrček, V.; Maguire, P.; Irvine, J. T. S.; Mariotti, D. Controlling the Energy-Level Alignment of Silicon Carbide Nanocrystals by Combining Surface Chemistry with Quantum Confinement. *J. Phys. Chem. Lett.* **2020**, *11* (5), 1721–1728.
- (15) Pringle, T. A.; Hunter, K. I.; Brumberg, A.; Anderson, K. J.; Fagan, J. A.; Thomas, S. A.; Petersen, R. J.; Sefannaser, M.; Han, Y.; Brown, S. L.; et al. Bright Silicon Nanocrystals from a Liquid Precursor: Quasi-Direct Recombination with High Quantum Yield. *ACS Nano* 2020, 14 (4), 3858–3867.
- (16) Sefannaser, M.; Thomas, S. A.; Anderson, K. J.; Petersen, R. J.; Brown, S. L.; Boudjouk, P. R.; Pringle, T. A.; Hobbie, E. K. Radiative Relaxation in Luminescent Silicon Nanocrystal Thiol-Ene Composites. *J. Phys. Chem. C* **2021**, *125* (10), 5824–5831.

- (17) Ortega-Liébana, M. C.; Hueso, J. L.; Arenal, R.; Lahoz, R.; de la Fuente, G. F.; Santamaría, J. Continuous-Mode Laser Ablation at the Solid-Liquid Interface of Pelletized Low-Cost Materials for the Production of Luminescent Silicon Carbide Nanocrystals. *J. Phys. Chem. C* 2015, 119 (4), 2158–2165.
- (18) Malone, W.; Nebgen, B.; White, A.; Zhang, Y.; Song, H.; Bjorgaard, J. A.; Sifain, A. E.; Rodriguez-Hernandez, B.; Freixas, V. M.; Fernandez-Alberti, S.; et al. NEXMD Software Package for Nonadiabatic Excited State Molecular Dynamics Simulations. *J. Chem. Theor. Comp.* **2020**, *16* (9), 5771–5783.
- (19) Wu, X.; Wen, S.; Song, H.; Frauenheim, T.; Tretiak, S.; Yam, C.; Zhang, Y. Nonadiabatic Molecular Dynamics Simulations Based on Time-Dependent Density Functional Tight-Binding Method. *J. Chem. Phys.* **2022**, *157* (8), No. 084114.
- (20) Chen, J.; Meng, Q.; Stanley May, P.; Berry, M. T.; Kilin, D. S. Time-Dependent Excited-State Molecular Dynamics of Photodissociation of Lanthanide Complexes for Laser-Assisted Metal-Organic Chemical Vapour Deposition. *Mol. Phys.* **2014**, *112* (3–4), 508–517.
- (21) Rabi, I. I. Space Quantization in a Gyrating Magnetic Field. Phys. Rev. 1937, 51 (8), 652-654.
- (22) Rabi, I. I.; Ramsey, N. F.; Schwinger, J. Use of Rotating Coordinates in Magnetic Resonance Problems. *Rev. Modern Phys.* **1954**, 26 (2), 167–171.
- (23) Tully, J. C. Molecular Dynamics with Electronic Transitions. *J. Chem. Phys.* **1990**, 93 (2), 1061–1071.
- (24) Han, Y.; Meng, Q.; Rasulev, B.; May, P. S.; Berry, M. T.; Kilin, D. S. Photofragmentation of the Gas-Phase Lanthanum Isopropylcy-clopentadienyl Complex: Computational Modeling vs Experiment. *J. Phys. Chem. A* **2015**, *119* (44), 10838–10848.
- (25) Han, Y.; Rasulev, B.; Kilin, D. S. Photofragmentation of Tetranitromethane: Spin-Unrestricted Time-Dependent Excited-State Molecular Dynamics. *J. Phys. Chem. Lett.* **2017**, *8* (14), 3185–3192.
- (26) Han, Y.; Meng, Q.; Rasulev, B.; May, P. S.; Berry, M. T.; Kilin, D. S. Photoinduced Charge Transfer versus Fragmentation Pathways in Lanthanum Cyclopentadienyl Complexes. *J. Chem. Theor. Comp.* **2017**, *13* (9), 4281–4296.
- (27) Erickson, M.; Han, Y.; Rasulev, B.; Kilin, D. Molecular Dynamics Study of the Photodegradation of Polymeric Chains. *J. Phys. Chem. Lett.* **2022**, *13* (19), 4374–4380.
- (28) Han, Y.; Anderson, K.; Hobbie, E. K.; Boudjouk, P.; Kilin, D. S. Unraveling Photodimerization of Cyclohexasilane from Molecular Dynamics Studies. *J. Phys. Chem. Lett.* **2018**, 9 (15), 4349–4354.
- (29) Forde, A.; Inerbaev, T. M.; Hobbie, E. K.; Kilin, D. S. Excited State Dynamics of a CsPbBr<sub>3</sub> Nanocrystal Terminated with Binary Ligands: Sparse Density of States with Giant Spin-Orbit Coupling Suppresses Carrier Cooling. *J. Am. Chem. Soc.* **2019**, *141* (10), 4388–4397.
- (30) Nelson, T. R.; White, A. J.; Bjorgaard, J. A.; Sifain, A. E.; Zhang, Y.; Nebgen, B.; Fernandez-Alberti, S.; Mozyrsky, D.; Roitberg, A. E.; Tretiak, S. Non-adiabatic Excited-State Molecular Dynamics: Theory and Applications for Modeling Photophysics in Extended Molecular Materials. *Chem. Rev.* **2020**, *120* (4), 2215–2287.
- (31) Levine, B. G.; Coe, J. D.; Virshup, A. M.; Martínez, T. J. Implementation of Ab Initio Multiple Spawning in the MOLPRO Quantum Chemistry Package. *Chem. Phys.* **2008**, 347 (1), 3–16.
- (32) Akimov, A. V.; Neukirch, A. J.; Prezhdo, O. V. Theoretical Insights into Photoinduced Charge Transfer and Catalysis at Oxide Interfaces. *Chem. Rev.* **2013**, *113* (6), 4496–4565.
- (33) Redfield, A. G. On the Theory of Relaxation Processes. *IBM J. Res. Dev.* **1957**, 1 (1), 19–31.
- (34) Kilin, D. S.; Micha, D. A. Relaxation of Photoexcited Electrons at a Nanostructured Si(111) Surface. *J. Phys. Chem. Lett.* **2010**, *1* (7), 1073–1077.
- (35) Huang, S.; Kilin, D. S. Charge Transfer, Luminescence, and Phonon Bottleneck in TiO<sub>2</sub> Nanowires Computed by Eigenvectors of Liouville Superoperator. *J. Chem. Theor. Comp.* **2014**, *10* (9), 3996–4005.

- (36) Inerbaev, T. M.; Han, Y.; Bekker, T. B.; Kilin, D. S. Mechanisms of Photoluminescence in Copper-Containing Fluoride Borate Crystals. *J. Phys. Chem. C* **2022**, *126* (14), 6119–6128.
- (37) O'Boyle, N. M.; Banck, M.; James, C. A.; Morley, C.; Vandermeersch, T.; Hutchison, G. R. Open Babel: An Open Chemical Toolbox. *J. Cheminf.* **2011**, *3*, 33.
- (38) SMARTS: A Language for Describing Molecular Patterns. https://www.daylight.com/dayhtml/doc/theory/theory.smarts.html (accessed 2023-04-15).

### **□** Recommended by ACS

## Effects of Ultraviolet Illumination on Oxygen Interstitial Injection from TiO<sub>2</sub> under Liquid Water

Heonjae Jeong and Edmund G. Seebauer

DECEMBER 01, 2022

THE JOURNAL OF PHYSICAL CHEMISTRY C

READ 🗹

#### Predictive Removal of Interfacial Defect-Induced Trap States between Titanium Dioxide Nanoparticles via Sub-Monolayer Zirconium Coating

Joyashish Debgupta, Richard E. Douthwaite, et al.

DECEMBER 23, 2022

THE JOURNAL OF PHYSICAL CHEMISTRY C

READ 🗹

#### Effect of Vacuum-Sealed Annealing and Ice-Water Quenching on the Structure and Photocatalytic Acetone Oxidations of Nano-TiO, Materials

Liping Wen, Baoshun Liu, et al.

NOVEMBER 17, 2022

ACS OMEGA

READ **C** 

#### Breaking Phonon Bottlenecks through Efficient Auger Processes in Perovskite Nanocrystals

Harry Baker, Patanjali Kambhampati, et al.

FEBRUARY 16, 2023

ACS NANO

READ 🗹

Get More Suggestions >